

Measuring quantum radiation reaction in laser–electron-beam collisions

T G Blackburn

Clarendon Laboratory, University of Oxford, Parks Road, Oxford, OX1 3PU, UK

E-mail: tom.blackburn@physics.ox.ac.uk

Abstract. Today’s high-intensity laser facilities produce short pulses can, in tight focus, reach peak intensities of 10^{22} Wcm $^{-2}$ and, in long focus, wakefield-accelerate electrons to GeV energies. The radiation-reaction–dominated regime, where the recoil from stochastic photon emission becomes significant, can be reached in the collision of such an electron beam with an intense short pulse. Measuring the total energy emitted in gamma rays or the presence of a prominent depletion zone in the electron beam’s post-collision energy spectrum would provide strong evidence of radiation reaction, provided enough electrons penetrate the region of highest laser intensity. Constraints on the accuracy of timing necessary to achieve this are given for a head-on collision.

PACS numbers: 41.60.-m, 52.38.Ph, 52.65.-y

Keywords: radiation reaction, colliding beams, strong-field QED

Submitted to: *Plasma Phys. Control. Fusion*

1. Introduction

The development of multi-PW laser systems, and the prospect of focussing laser pulses to intensities greater than 10^{22} Wcm $^{-2}$ [1, 2], has led to substantial interest in how radiation reaction and strong-field quantum electrodynamics (QED) processes will alter the plasma physics studied over the next decade. Future laser systems will be powerful enough such that the high fluxes of gamma rays (i.e. photons in the MeV range) and electron-positron pairs they produce in laser–laser [3, 4, 5] and laser–solid [6, 7] interactions exert significant feedback on the evolution of the plasma, increasing the absorption of laser energy [14]. It will become possible to test the physics underpinning exotic astrophysical phenomena, e.g. pair cascades in pulsar magnetospheres [8, 9], and illuminate fundamental questions about radiation reaction and the quantum vacuum in QED [10].

The importance of strong-field QED effects may be quantified with the parameter

$$\eta = \frac{|F_{\mu\nu}p^\nu|}{mcE_{\text{Sch}}} \quad (1)$$

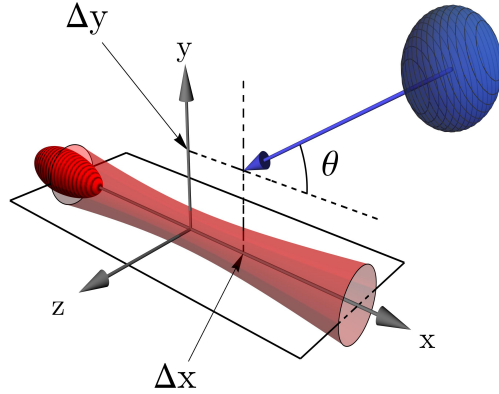


Figure 1. The experimental configuration under consideration: a GeV electron beam (blue) colliding with an laser pulse of intensity 10^{22} Wcm^{-2} (red). The laser moves in the positive x -direction; the electron beam centre is located in, and the electrons' initial momenta are parallel to, the x - y plane. Observing radiation reaction will depend upon the degree to which the beams overlap, i.e. the collision timing and angle θ . The timing error is parameterised by $(\Delta x, \Delta y)$, the location of the electron beam centre at $t = 0$, when the laser pulse is focussed at the origin. We do not consider the effects of a displacement between the beams in the z -direction.

where $F_{\mu\nu}$ is the electromagnetic field tensor and $p^\mu = \gamma m(c, \mathbf{v})$ the electron four-momentum [3]. (This parameter is also called χ [11] or χ_e [12].) η compares the magnitude of the electric field in the electron's rest frame to that of the critical field of QED $E_{\text{Sch}} = 1.3 \times 10^{16} \text{ Vcm}^{-1}$, which can produce electron-positron pairs directly from the vacuum [13].

η also controls the stochasticity of photon emission. As the typical energy of a radiated photon for $\eta < 1$ is $\hbar\omega \simeq 0.44\eta\gamma mc^2$ [3], when $\eta \simeq 1$, an electron can lose a substantial fraction of its energy in a single emission. Radiation reaction must be then treated as stochastic, rather than as the continuous loss of energy predicted classically. Pair production can become significant in laser–solid interactions [6, 7] for $\eta \sim 1$; in a colliding beams experiment, where the electron is not reaccelerated by the laser, $\eta \gg 1$ is required for these processes to be significant [12, 14].

For highly relativistic electrons, (1) becomes

$$\eta \simeq \frac{\gamma |\mathbf{E}_\perp + \mathbf{v} \times \mathbf{B}|}{E_{\text{Sch}}} \quad (2)$$

where γ is the electron Lorentz factor, \mathbf{B} the magnetic field and \mathbf{E}_\perp the electric field component perpendicular to \mathbf{v} . In a laser–plasma interaction we would expect the electrons to have $\gamma \simeq a_0$, where $a_0 = [I(\lambda/\mu\text{m})^2/1.37 \times 10^{18} \text{ Wcm}^{-2}]^{1/2}$ is the laser's strength parameter, I its intensity and λ its wavelength. Then the typical $\eta \simeq I\lambda/(5.65 \times 10^{23} \text{ Wcm}^{-2}\mu\text{m})$ and intensities $> 10^{23} \text{ Wcm}^{-2}$ would be necessary to observe strong-field QED effects.

However, if the electrons are pre-accelerated to high energies before encountering the high field region, the QED-dominated regime can be reached using much lower laser intensities. This was exploited in experiment E-144 at the SLAC facility [15, 16], in which the collision of a 46.6 GeV electron beam and laser pulse of intensity 10^{18} Wcm^{-2} was observed to produce electron-positron pairs by photon–photon scattering. The advent of wakefield-accelerated electron beams with energies of

1 GeV [18, 19] or greater [20, 21] and intense short pulses [26] now raises the possibility that this experiment could be repeated with an all-optical setup in today’s laser facilities. This has already been accomplished for target laser pulses with $a_0 \simeq 1$ [22, 23]; recently Sarri *et al* [24] demonstrated production of multi-MeV gamma rays by non-linear Thomson scattering of a ~ 400 MeV electron beam. If high- Z solid rather than a laser pulse is used as a target, wakefield-accelerated electron beams can also be used to generate dense electron-positron plasmas by bremsstrahlung [25].

For collisions at $a_0 \simeq 1$, the electron recoil is negligible. However, for a GeV electron beam and laser pulse of intensity 10^{22} Wcm $^{-2}$, $\eta \simeq 1$ and quantum radiation reaction will dominate the dynamics of the electron beam. There is now a large body of work considering how strong-field QED effects can be observed in the spectra of the emitted gamma rays and the electron beam of such an experiment [27, 28, 29, 30, 31, 32, 33].

In previous work [34], we considered the collision of a GeV electron beam with a laser pulse of intensity 10^{21} to 3×10^{22} Wcm $^{-2}$; the beams collided at an angle of 180° and were timed to coincide perfectly at the laser focus. Quantum radiation reaction could be experimentally diagnosed by measuring the increased yield of high-energy gamma rays or the reduced energy of the electron beam after the collision.

Both these signatures are sensitive to the overlap between the electron beam and laser pulse, which places constraints on the accuracy of collision timing required. In this article we will consider how the collision timing, and the angle between the beams, affects the total gamma ray energy, the electron beam’s final energy spectrum and therefore the viability of diagnosing quantum radiation reaction in an experiment using today’s high intensity laser facilities.

Section 2 describes the algorithm by which these interactions are simulated; section 3 describes the chosen experimental parameters of GeV electron beam and 10^{22} Wcm $^{-2}$, 30 fs laser pulse. Section 4 presents simulated gamma ray spectra and shows that the yield is maximised in a head-on collision that occurs 80 μm from the laser focal spot. Section 5 presents simulated electron spectra and shows that, if the collision is accurate enough, radiation reaction leads to a substantial energy loss in that part of the electron beam the laser passes through. As measuring that loss can be a robust signature of radiation reaction, we constrain how accurate a collision must be for it to be sufficiently large.

2. Method of simulation

The collision of a GeV electron beam with a laser pulse of intensity 10^{22} Wcm $^{-2}$ is simulated with a single-particle, Monte-Carlo code that includes the electron’s oscillatory motion in the laser fields and the strong-field QED process of synchrotron photon emission. As pair production by the resulting gamma rays is likely to be negligible for these parameters [34], we can neglect it here.

Following [35, 36, 37], the differential rate of photon emission is

$$\frac{d^2N}{dt d\chi} = \frac{\sqrt{3}\alpha}{2\pi\tau_C} \frac{\eta}{\gamma} \frac{F(\eta, \chi)}{\chi}. \quad (3)$$

$\chi = \hbar|F_{\mu\nu}k^\nu|/2mcE_{\text{Sch}}$, where the four-frequency $k^\mu = (\omega/c, \mathbf{k})$, is the equivalent of η for the photon; the Compton time $\tau_C = \hbar/mc^2$ and the quantum synchrotron function, discussed in Appendix A, is defined for $0 \leq \chi \leq \eta/2$. Integrating (3) over

that range gives the total rate of emission $dN/dt \propto \eta h(\eta)/\gamma$, where the function

$$h(\eta) = \int_0^{\eta/2} \frac{F(\eta, \chi)}{\chi} d\chi \quad (4)$$

is a monotonically decreasing function of η that satisfies $\lim_{\eta \rightarrow 0} h(\eta) = 5\pi/3$.

This rate is calculated in the Furry picture of QED [38], including an external, unquantised electromagnetic field. The basis states derived for this field may be used to calculate Feynman rules for quantised interactions [39, 40, 41].

Where the photon formation length is much smaller the characteristic length of the fields, that emission may be treated as pointlike and the fields quasistatically; thus the rate can be calculated in an equivalent system that has the same value of η . As the photon formation length $L_{\text{ph}} = \lambda/a_0$ [4], we may treat the laser fields as quasistatic provided $a_0 \gg 1$. In Erber [35], the equivalent system used to derive (3) is a static magnetic field in the limit $B \rightarrow 0$, $\gamma \rightarrow \infty$.

The emission algorithm follows the work of [5, 6, 34, 42] and is similar to that described in [32, 43]. Photon emission is a stochastic process and governed by Poisson statistics; the probability P of emission in a field with optical depth τ is $P = 1 - e^{-\tau}$. At the start of the simulation, and following each emission, the electron is assigned a ‘final’ optical depth $\tau_f = -\log(1 - P)$ for pseudorandom $P \in [0, 1]$. The electron’s optical depth τ is integrated along its trajectory until τ_f is reached, according to

$$\frac{d\tau}{dt} = \int_0^{\eta/2} \frac{d^2N}{dt d\chi} d\chi = \frac{\sqrt{3}\alpha}{2\pi\tau_C} \frac{\eta}{\gamma} h(\eta). \quad (5)$$

At this point, the photon energy $\hbar\omega = 2\chi mc^2/\eta$ is selected by solving

$$r h(\eta) = \int_0^{\chi} \frac{F(\eta, \chi')}{\chi'} d\chi' \quad (6)$$

for χ , where the pseudorandom number r is uniformly distributed in $[0, 1]$. The electron then recoils antiparallel to its motion, with change of momentum $\hbar\omega/c$. Energy conservation therefore requires that a small amount of energy is transferred from the laser fields during emission; as described in [5], this leads to a fractional error in the electron energy of $\Delta\gamma/\gamma \propto 1/\gamma$ that may be safely neglected. While synchrotron radiation is directed forward into a cone of opening angle $\sim 1/\gamma$ [44], we can assume that the photon and electron momenta are collinear, as the electron is always highly relativistic.

Between emissions, the electron trajectory is determined classically by integrating the Lorentz force exerted by the laser fields (neglecting the beam’s space charge field, as described in section 3.2)

$$\frac{d\mathbf{r}}{dt} = \frac{\mathbf{p}}{\gamma m} \quad (7)$$

$$\frac{d\mathbf{p}}{dt} = -e(\mathbf{E} + \mathbf{v} \times \mathbf{B}). \quad (8)$$

This is implemented using a Boris push algorithm [45], so \mathbf{E} and \mathbf{B} are calculated at intervals staggered by half a timestep.

The electron trajectories are discretised into timesteps of 0.005 fs, and at least 10^7 trajectories are followed for each set of parameters.

3. Parameters

A schematic of the experimental configuration under consideration is given in figure 1. We consider varying the angle of collision θ as well as the mistiming in the x - y plane. This is parameterised by the offsets $(\Delta x, \Delta y)$, which correspond to the displacement of the electron beam centre from the origin at $t = 0$, at which time the laser is focussed there.

3.1. Laser pulse

The laser is a Gaussian focussed beam with waist $w_0 = 2 \mu\text{m}$ and wavelength $\lambda = 0.8 \mu\text{m}$, linearly polarised along the y axis and propagating towards $+x$. It has a Gaussian temporal intensity profile with maximum $I = 10^{22} \text{Wcm}^{-2}$ ($a_0 = 65$) and full length at half maximum $f = c \cdot 30 \text{fs} = 9 \mu\text{m}$. The peak field E_0 is related to the laser intensity by $I = \frac{1}{2}c\epsilon_0 E_0^2$.

It can be shown from (2) that η , which controls photon emission, does not depend on the polarisation of the EM field, but only on the angle between the optical axis and the electron momentum θ . As such, the choice of polarisation here is arbitrary except that it defines the plane in which the electrons oscillate and so affects the angular distribution of radiation. This will be a fan of opening angle $\sim a_0/\gamma$ oriented along the polarisation axis [34].

3.2. Electron beam

The energy distribution of the electron beam (up to a normalising constant) is

$$\frac{dN}{d\mathcal{E}} \propto (\mu + \sigma/3 - \mathcal{E})^{-3/2} \exp\left(-\frac{\sigma}{2(\mu + \sigma/3 - \mathcal{E})}\right) \quad (9)$$

for $100 \text{ MeV} \leq \mathcal{E} \leq \mu + \sigma/3$; it has a peak at $\mu = 1000 \text{ MeV}$ and a width σ of 250 MeV , which is related to the full width at half maximum (fwhm) f by $f = 0.9\sigma$. This is shown in figure 4. This distribution has been chosen as high energy wakefield-accelerated beams typically have large tails that extend to low energy. They also exhibit an angular divergence of order mrad, but here their initial momenta are directed along $\hat{\mathbf{p}}_0 = -(\cos \theta, \sin \theta, 0)$.

The charge density of the beam forms a Gaussian envelope with $\sigma_{\parallel} = 3.8 \mu\text{m}$ and $\sigma_{\perp} = 4.2 \mu\text{m}$ ($\text{fwhm}_{\parallel} = 9 \mu\text{m}$ and $\text{fwhm}_{\perp} = 10 \mu\text{m}$) where the widths are given in the directions parallel and perpendicular to $\hat{\mathbf{p}}_0$ respectively.

The electric and magnetic components of the space charge force $F_{\text{sc}} \simeq Qe/(\gamma^2\epsilon_0\sigma_{\perp}^2)$ of an electron bunch that has cylindrical symmetry nearly cancel if the electrons are ultrarelativistic $\gamma \gg 1$. The force of radiation reaction $F_{\text{rr}} \simeq \alpha\eta^2 mc/\tau_C$ [3]. For $Q \simeq 100 \text{ pC}$, $\sigma_{\perp} \simeq 4 \mu\text{m}$ and $\eta \simeq 0.1$, $F_{\text{sc}} \ll F_{\text{rr}}$ means that the effect of the space charge field can be neglected and each electron's trajectory in the laser pulse may be considered separately.

Furthermore, as the typical separation between electrons $(\sigma_{\parallel}\sigma_{\perp}^2 e/Q)^{1/3} \simeq 5 \text{ nm}$ (equivalent to 40 eV), we can also neglect collective radiation effects when considering gamma ray emission.

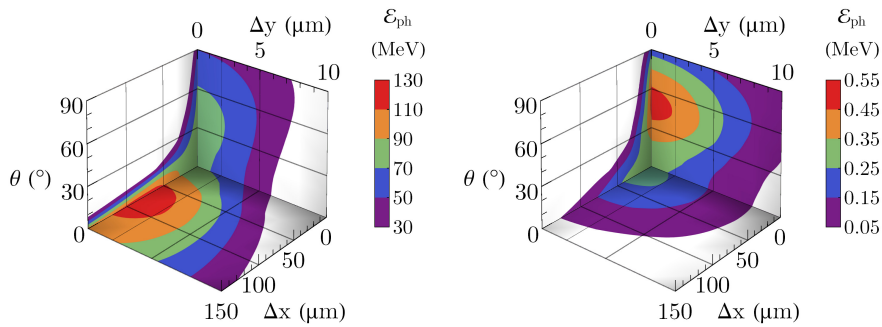


Figure 2. The energy radiated by a GeV electron beam, per electron, to photons of all energies (left) and to photons with $\hbar\omega > 500$ MeV (right), when colliding with a Gaussian laser pulse of intensity 10^{22} Wcm^{-2} at an angle θ with parallel and perpendicular offsets Δx and Δy .

4. Gamma ray production

We consider the interaction of an intense laser pulse with a GeV electron beam, with parameters as described in section 3.2. Figure 2 shows the mean energy lost by such an electron beam to gamma rays when colliding with the specified laser pulse.

We find that the total loss reaches its maximum of 120 MeV per electron for a head-on collision that occurs a distance $\Delta x = 80 \mu\text{m}$ along the optical axis from the laser focus, but that the loss to photons with energy > 500 MeV is maximised at 0.48 MeV per electron for a perfectly-timed collision that occurs at an angle of 50° .

In determining the $(\Delta x, \Delta y, \theta)$ that maximise the energy emitted to gamma rays, we must consider three competing factors: a) the geometric factor in η ; b) each electron’s length of interaction with the laser pulse; and c) the overlap between the electron beam and laser pulse.

a) arises from the definition of η (2): if \mathbf{E} and \mathbf{B} are given by a linearly polarised plane wave and the electron is highly relativistic, travelling at angle θ to the wave’s direction of propagation, then

$$\eta = \frac{\gamma|\mathbf{E}_\perp + \mathbf{v} \times \mathbf{B}|}{E_{\text{Sch}}} = \frac{\gamma(1 + \cos\theta)|\mathbf{E}|}{E_{\text{Sch}}}. \quad (10)$$

As η falls with increasing θ , colliding the electron with the laser pulse at an angle will have two effects: according to (5) the electron’s emission rate is reduced; and the photons it emits have lower energies, as the tail of the synchrotron spectrum grows non-linearly with increasing η .

b) accounts for the importance of ‘straggling’ [5]: as photon emission is probabilistic, some electrons can reach the centre of the laser pulse having lost no energy; their η is then much higher and so too their probability of emitting a single photon with $\hbar\omega \sim \gamma mc^2$. In this case, the laser pulse is longer along the propagation axis than it is wide, so electrons traversing the pulse at an angle interact with the high intensity field over a shorter distance. While this reduces the total energy emitted, straggling becomes likelier with a shorter distance to reach the region of highest intensity; this should increase the yield of the highest energy photons.

We can see the interplay of these two factors in the yield of the highest energy gamma rays, which is maximised for a collision at 50° rather than at 0° . This can be

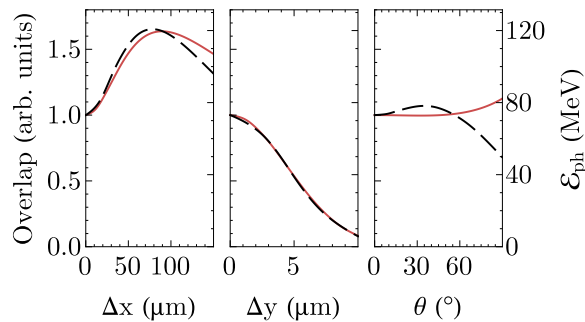


Figure 3. The overlap between the laser pulse and electron beam (red, solid: left scale), normalised to the overlap at $\Delta x = \Delta y = \theta = 0$, and the total loss of energy to photons per electron (black, dashed: right scale), varying only Δx (left), Δy (centre) and θ (right).

explained by estimating analytically the average η of an electron when it emits its first photon, which balances the reduced geometric factor against increased penetration into the laser pulse as θ increases. The latter is likely to be more important than both the geometric factor and the overlap between the beams as it is the emission of the highest energy photons that is most sensitive to straggling [34]. The calculation is given in Appendix B; for the parameters under consideration here, η is maximised for a collision $\theta = 65^\circ$, which is consistent with the peak shown in the right of figure 2. We conclude that it is most important to reduce the length of interaction and so the energy loss in the foot of the pulse to maximise the yield of the highest energy photons.

However, maximising the total yield of gamma rays is achieved for a head-on collision at $\Delta x = 80\mu\text{m}$. We can understand this in terms of c), the overlap, which controls how many of the beam electrons interact with the laser pulse. Let us compare the total energy emitted in photons to an analytical estimate of the overlap

$$\Omega = \int dt \int d^3\mathbf{r} \rho(\mathbf{r}, t) |E(\mathbf{r}, t)| \quad (11)$$

where the beam charge density is as given in section 3.2 and $|E(\mathbf{r}, t)|$ is as given in section 3.1, taking $|\sin \phi| = 2/\pi$. That comparison is plotted in figure 3, varying each of Δx , Δy and θ .

We can see that the overlap models the dependence of the yield on Δx and Δy well. The yield increases with Δx up to $\Delta x = 80\mu\text{m}$ because the laser pulse diverges as it propagates away from its focal plane and therefore more electrons encounter the pulse. For $\Delta x > 80\mu\text{m}$ the yield falls because even though more electrons collide with the laser, they do so at lower peak intensity, which reduces their η and so their emissivity.

Gamma ray production is more sensitive to the perpendicular displacement between the beams Δy than the parallel displacement Δx . This is because the peak intensity at the electron beam centre falls as $\exp(-2(\Delta y/w_0)^2)$ for increasing Δy but as $[1 + (\Delta x/x_R)^2]^{-1}$ for increasing Δx ; to reduce the peak intensity by a half requires $\Delta x = 16\mu\text{m}$ but only $\Delta y = 1.4\mu\text{m}$. For $\Delta y > 10\mu\text{m}$ there is negligible photon emission because nearly all the electrons have missed the laser pulse.

The overlap between the beams is nearly constant if only θ is varied; however, the gamma ray yield is maximised at 80 MeV per electron at $\theta = 35^\circ$ and falls thereafter.

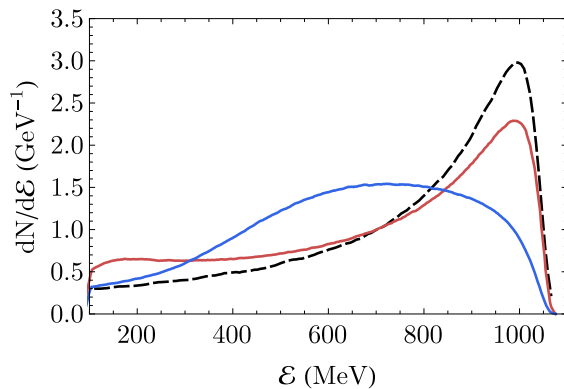


Figure 4. The energy spectrum of the electron beam before the collision (black, dashed) and after a collision at $\Delta x = 0$ (red) and $90 \mu\text{m}$ (blue).

We can attribute this behaviour to the reduced length of interaction at large θ , which reduces the energy loss before the electron reaches the pulse centre. However, this does not increase the gamma ray yield as much as increasing Δx .

We conclude that allowing the laser pulse to diverge over a distance of $80 \mu\text{m}$ in a head-on collision is the optimal configuration to produce gamma rays. This can be achieved experimentally by focussing the high-intensity laser pulse with an optic that has an aperture in it. Provided this aperture is of sufficient size to permit the transmission of the wakefield-driving laser, the electron beam and resultant gamma rays, back-reflection and damage to the optical chain can be avoided.

An analytical fit to the region in which the total gamma ray yield is at least 80% of its maximum value is

$$\left(\frac{\Delta x - 91 \mu\text{m}}{60 \mu\text{m}}\right)^2 + \left(\frac{\Delta y}{3.6 \mu\text{m}}\right)^2 \leq 1 \quad (12)$$

for $\theta = 0^\circ$. Even though the experiment would be designed for counterpropagation, the angle between the beams will vary from shot to shot due to the pointing variation of both the wakefield-driving and target laser pulses. Figure 2 shows that to achieve any gamma ray production at $\Delta x = 80 \mu\text{m}$, that angle must be less than 15° . We can understand this requirement by considering the distance of closest approach between the centres of the electron beam and laser pulse $\Delta_{\text{min}} = \Delta x \sin \theta / 2$; for $\Delta x = 80 \mu\text{m}$, $\theta > 15^\circ$ means $\Delta_{\text{min}} > 10 \mu\text{m}$, the width of the electron beam, and so there is no overlap between the beams.

5. Energy loss of the electron beam

Detecting radiation reaction in an experiment could also be accomplished by comparing the energy spectrum of a wakefield-accelerated electron beam with and without the target short pulse, showing the reduced energy of the beam in the former case. Figure 4 compares the energy distribution of the GeV electron beam described in section 3.2 to its initial energy spectrum for collisions at $\Delta x = 0$ and $90 \mu\text{m}$.

We can see in that in the former case the spectra are not sufficiently distinguishable, even though there is substantial loss of energy to gamma rays. That

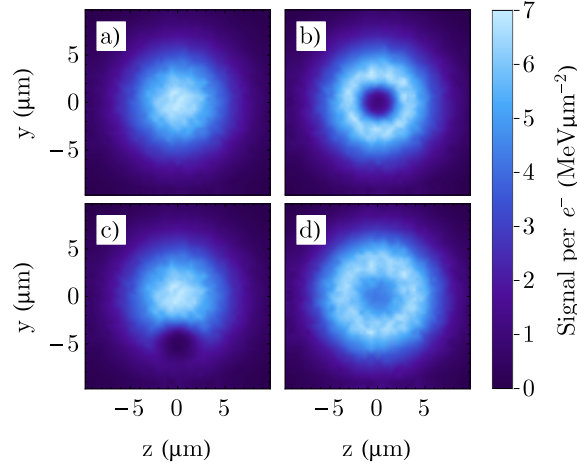


Figure 5. The energy carried by the electron beam, per electron, per unit cross-sectional area a) prior to the collision and immediately after a collision at b) $\Delta x = \Delta y = 0$, c) $\Delta x = 0$, $\Delta y = 5 \mu\text{m}$ and d) $\Delta x = 50 \mu\text{m}$, $\Delta y = 0$.

loss is generated by those electrons that have collided with the intense part of the laser pulse; however, the peak at 1000 MeV remains as many electrons miss the laser pulse entirely. The broad energy spread is caused not only by the range of peak intensities encountered by the electron beam but by the stochastic nature of emission as well: two electrons travelling along the same trajectory will not necessarily lose the same energy. Neitz and Di Piazza [28] showed that this leads to energy broadening even for an electron beam without spatial extent and that radiation reaction manifests itself by ‘smearing out’ the initial energy distribution.

If we consider the final state energy distribution for a collision at $\Delta x = 90 \mu\text{m}$, enough of the beam interacts with the laser such that the initial peak at 1000 MeV is entirely removed. If the electron beam is sufficiently well-characterised, it may be possible to detect radiation reaction by comparing the spectra from shots in the presence and absence of the target laser pulse. However, even high-quality wakefield-accelerated electron beams do not in general have energy spectra that are reproducible from shot to shot. An imperfectly generated electron beam would be a plausible origin of the blue spectrum in figure 4.

An alternative method of diagnosing radiation reaction exploits the fact that the laser pulse has a smaller diameter than the electron beam. Figure 6 shows the energy carried by the electron beam over its cross-sectional area, i.e. its energy per unit volume integrated along its direction of propagation, for electrons that have collided with the laser pulse for various $(\Delta x, \Delta y, \theta)$. We can see by comparing a) and b) that the laser pulse causes significant depletion of the energy spectrum in a region of radius $2 \mu\text{m}$ around the optical axis. Resolving the electron’s beam areal energy spectrum could be accomplished by allowing to diverge over a long distance as it propagates away from the interaction region. A single shot would thereby allow the simultaneous measurement of the electron beam energy in the presence and absence of the target laser pulse and so the detection of radiation reaction.

If we introduce a perpendicular displacement between the beams $\Delta y = 5 \mu\text{m}$,

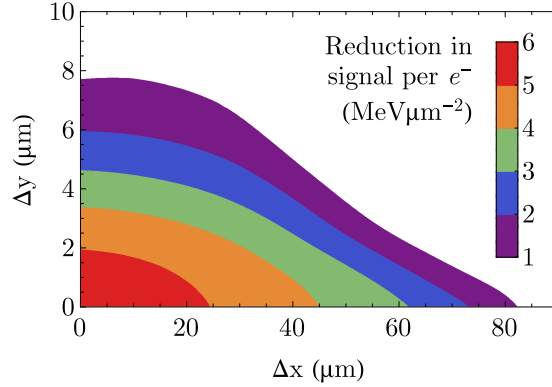


Figure 6. The reduction in the energy carried by the electron beam per unit cross-sectional area, at the point where the laser pulse passes through the beam.

as in c), the depletion zone is still evident. However, d) shows that a longitudinal displacement, which allows the laser pulse to broaden before the collision takes place, makes the depletion zone less obvious. This is because the laser interacts with more electrons but at lower peak intensity, spreading the energy loss over a larger region of the electron beam. By considering the amount by which the energy is reduced at the centre of the depletion zone for collisions that take place at $\theta = 0^\circ$, as in figure 6, we can constrain the accuracy of collision necessary for the depletion zone to be evident. An analytical fit to the region in which that loss $> 3 \text{ MeV}\mu\text{m}^{-2}$ is

$$\frac{\Delta y}{4.6 \mu\text{m}} + \left(\frac{\Delta x}{61 \mu\text{m}}\right)^2 \leq 1. \quad (13)$$

6. Conclusions

The gamma ray yield and the energy loss of the electron beam are sensitive to both the maximal η reached by the electrons as well as the length over which this is sustained. However, for a realistic electron beam, the overlap between the beams will be a more significant factor in determining the strength of radiation reaction.

Maximising these requires the counterpropagation of the electron beam and laser pulse; this exploits the slow angular divergence of the laser pulse, minimising the accuracy of longitudinal timing required, and the geometric factor $(1 + \cos \theta)$ in η .

For a GeV electron beam colliding head-on with a 30 fs laser pulse of intensity 10^{22} Wcm^{-2} , the mean energy lost to gamma rays will be maximised at 120 MeV per electron for a collision that occurs $80 \mu\text{m}$ along the optical axis from the laser focal plane. If the collision occurs closer to the focal spot, the gamma ray yield is reduced, but there will be a prominent depletion zone in the areal energy spectrum of the electron beam.

The total energy emitted to gamma rays will be at least 80% of its maximum if the parallel and perpendicular offsets satisfy

$$\left(\frac{\Delta x - 91 \mu\text{m}}{60 \mu\text{m}}\right)^2 + \left(\frac{\Delta y}{3.6 \mu\text{m}}\right)^2 \leq 1 \quad (14)$$

and the depletion zone in the electron spectrum will be significant, i.e. the areal energy will be reduced by more than $3 \text{ MeV}\mu\text{m}^{-2}$ from its unperturbed value, if

$$\frac{\Delta y}{4.6 \mu\text{m}} + \left(\frac{\Delta x}{61 \mu\text{m}}\right)^2 \leq 1. \quad (15)$$

The latter allows the simultaneous measurement of the electron beam energy in the presence and absence of the laser pulse and so the detection of radiation reaction.

A head-on collision can be accomplished by focussing the high-intensity target laser pulse using an optic with an aperture of sufficient size to permit the transmission of the wakefield-driving laser, the electron beam and resultant gamma rays. Obtaining a Δx and Δy that satisfy the accuracy requirements (14) and (15) will rely on gathering statistics over a large series of laser shots. While the region in $\Delta x, \Delta y$ phase space is small, the energy converted to gamma rays will be sufficiently large, and the resulting depletion zone in the electron spectrum sufficiently prominent, to be robust signatures of radiation reaction for experimental parameters that can be achieved in current high intensity laser facilities.

Acknowledgments

This work was supported by an EPSRC studentship. The author thanks A.R. Bell and C.P. Ridgers for continued advice and support.

Appendix A. The quantum synchrotron function

The quantum synchrotron function is

$$F(\eta, \chi) = \frac{4\chi}{3\eta^2} \left[\left(1 - \frac{2\chi}{\eta} + \frac{1}{1 - 2\chi/\eta}\right) K_{2/3}(\delta) - \int_{\delta}^{\infty} K_{1/3}(t) dt \right] \quad (A.1)$$

where

$$\delta = \frac{4\chi}{3\eta^2} \left(1 - \frac{2\chi}{\eta}\right)^{-1}. \quad (A.2)$$

For small χ , this is approximately

$$F(\eta, \chi) = \left(\frac{16}{3}\right)^{1/3} \Gamma\left(\frac{2}{3}\right) \eta^{-2/3} \chi^{1/3}. \quad (A.3)$$

This means that $F(\eta, \chi)/\chi$, and so the differential rate of photon emission (3), diverge as $\chi^{-2/3}$ for low frequencies. However, the normalised energy emitted to photons with frequency between χ and $\chi + d\chi$ during interval dt , $\chi \frac{d^2 N}{dt d\chi} dt d\chi$, is well defined for all χ . In particular, it is zero for $\chi = 0$. Similarly, the total rate of photon emission (5), which depends on $\int F(\eta, \chi)/\chi d\chi$, is always well defined.

Appendix B. The typical η of an electron emitting its first photon

Recalling that

$$\eta = \frac{\gamma |\mathbf{E}_{\perp} + \mathbf{v} \times \mathbf{B}|}{E_{\text{Sch}}} = \frac{\gamma(1 + \cos \theta) |\mathbf{E}|}{E_{\text{Sch}}} \quad (B.1)$$

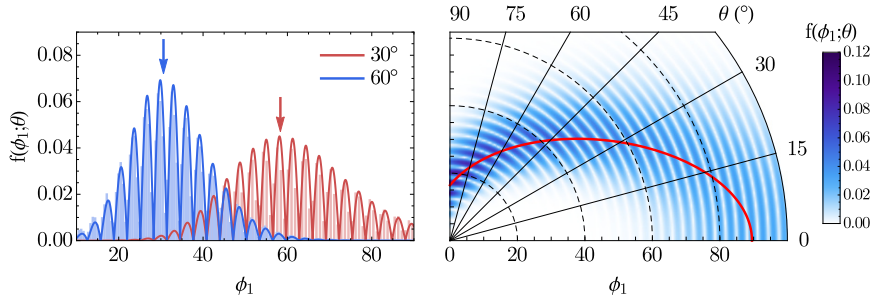


Figure B1. (left) The probability density that an electron colliding with Gaussian laser pulse of intensity 10^{22} Wcm^{-2} at $\theta = 30^\circ$ (red) and 60° (blue) emits its first photon at wave phase ϕ_1 . The curves are calculated using (B.8) and the vertical bars give the distribution found in simulations for a single electron with $\mathcal{E}_0 = 1000$ MeV colliding with a laser pulse as described in section 3.1. The arrows indicate the value of $\phi_{1,mp}$ given by (B.9). (right) Density plot of $f(\phi_1; \theta)$: the red line is $\phi_{1,mp}$.

for an ultrarelativistic electron propagating at angle θ to a linearly polarised electromagnetic wave, the rate of change of optical depth against emission is

$$\frac{d\tau}{dt} = \frac{\sqrt{3}\alpha}{2\pi\tau_C} \frac{\eta}{\gamma} h(\eta) = \frac{\sqrt{3}\alpha}{2\pi\tau_C} (1 + \cos\theta) \frac{|E(t)|}{E_{\text{Sch}}} h(\eta). \quad (\text{B.2})$$

The first approximation is that $h(\eta) \simeq h(0) = 5\pi/3$ at all times along the electron trajectory. This is justified as in the foot of the pulse, the electric field is sufficiently small to keep $\eta \lesssim 0.1$. Even then, $h(0.1) = 0.93h(0)$ so any overestimate of the rate will be negligible.

In the presented simulations, $\mathcal{E}_0 = 1000$ MeV and therefore the electron can be treated as ultrarelativistic. Therefore its initial momentum is $\mathbf{p}_0 = -\mathcal{E}_0/c(\cos\theta, \sin\theta, 0)$. As $\gamma_0 = \mathcal{E}_0/m_e \gg a_0$, it can be assumed that any deflection of the electron by the laser pulse is minimal. Its trajectory before emission is linear, with position at time t given by $(x, y, z) = -ct(\cos\theta, \sin\theta, 0)$. As (B.2) depends on the electron energy only through $h(\eta)$, which we have approximated as constant, the result will depend on \mathcal{E}_0 only in the sense that it must be sufficiently large that the electron be ultrarelativistic.

In the simulations the full form of the Gaussian beam was used. However, for simplicity in these calculations, neglecting wavefront curvature and beam divergence gives

$$E = E_0 \sin\phi \exp\left(-\frac{y^2 + z^2}{w_0^2} - \frac{2 \ln 2 \phi^2}{k^2 f^2}\right) \quad (\text{B.3})$$

$$\phi = kx - \omega t = -(1 + \cos\theta)\omega t \quad (\text{B.4})$$

where ω is the laser's angular frequency, k its wavevector, w_0 its waist size and f the full length at half maximum of its temporal intensity profile.

Using (B.4) to recast (B.2) and (B.3) in terms of ϕ , we find

$$\frac{d\tau}{d\phi} = -\frac{5\alpha}{2\sqrt{3}\omega\tau_C} \frac{E_0}{E_{\text{Sch}}} |\sin\phi| \exp(-\zeta^2 \phi^2) \quad (\text{B.5})$$

where

$$\zeta^2 = \frac{\sin^2\theta}{(1 + \cos\theta)^2 k^2 w_0^2} + \frac{2 \ln 2}{k^2 f^2}. \quad (\text{B.6})$$

As the envelope in (B.5) varies slowly with ϕ , we can approximate the oscillatory factor $|\sin \phi| \simeq 2/\pi$ and thus integrate (B.5) from ∞ to ϕ_1 , the wave phase at which the electron emits its first photon. We find the following relation between the final optical depth and ϕ_1 :

$$\tau_f \simeq \frac{5\alpha}{2\sqrt{3}\pi\omega\tau_C} \frac{E_0}{E_{\text{Sch}}} \frac{1 - \text{erf}(\zeta\phi_1)}{\zeta}. \quad (\text{B.7})$$

Photon emission is a stochastic process and governed by Poisson statistics, so these final optical depths are distributed as $\tau_f \sim \exp(-\tau_f)$. Then the probability density that an electron colliding with a Gaussian laser pulse at angle θ emits its first photon at phase ϕ_1 is given by

$$f(\phi_1; \theta) = \exp(-\tau_f) \left| \frac{d\tau_f}{d\phi} \right| \quad (\text{B.8})$$

where we substitute (B.7) in the exponent and (B.5) in the modulus. Figure B1 compares the analytical $f(\phi_1; \theta)$ with that obtained from simulation and finds good agreement.

It is evident from figure B1 that at larger angles of collision, the electron is more likely to penetrate further into the laser pulse before emitting its first photon; both the peak and the width of the distribution decrease as θ grows, reducing the length of interaction. The most probable $\phi_1 = \phi_{1,\text{mp}}$ can be estimated by solving $df(\phi_1; \theta)/d\phi_1 = 0$, using (B.7), to find

$$\phi_{1,\text{mp}}^2 \simeq \frac{1}{2\zeta^2} W \left[\frac{1}{\zeta^2} \left(\frac{5\alpha}{\sqrt{6}\pi} \frac{1}{\omega\tau_C} \frac{E_0}{E_{\text{Sch}}} \right)^2 \right] \quad (\text{B.9})$$

where $W(x)$ is the Lambert W function, defined by $x = W(x)e^{W(x)}$, and ζ^2 is as given in (B.6).

We can substitute (B.9) into $|\mathbf{E}| \simeq E_0 \exp(-\zeta^2\phi^2)$ and then $\eta = \gamma(1 + \cos\theta)|\mathbf{E}|/E_{\text{Sch}}$ to arrive at an estimate of the typical η of an electron emitting its first photon:

$$\eta \simeq \frac{\gamma_0(1 + \cos\theta)E_0}{E_{\text{Sch}}} \exp(-\zeta^2\phi_{1,\text{mp}}^2). \quad (\text{B.10})$$

For a GeV electron colliding with the laser pulse described in section 3.1, it is maximised for $\theta = 65^\circ$.

References

- [1] The Vulcan 10 PW Project <http://www.stfc.ac.uk/CLF/Facilities/Vulcan/14684.aspx>
- [2] The Extreme Light Infrastructure (ELI) Project <http://www.eli-beams.eu/>
- [3] Bell A R and Kirk J G 2008 *Phys. Rev. Lett.* **101** 200403
- [4] Kirk J G, Bell A R and Arka I 2009 *Plasma Phys. Control. Fusion* **51** 085008
- [5] Ducloux R, Kirk J G and Bell A R 2011 *Plasma Phys. Control. Fusion* **53** 015009
- [6] Ridgers C P, Brady C S, Ducloux R, Kirk J G, Bennett K, Arber T D, Robinson A P L and Bell A R 2012 *Phys. Rev. Lett.* **108** 165006
- [7] Brady C S, Ridgers C P, Arber T D, Bell A R and Kirk J G 2012 *Phys. Rev. Lett.* **109** 24006
- [8] Goldreich P and Julian W H 1969 *Astrophys. J.* **157** 869
- [9] Timokhin A N 2010 *Mon. Not. R. Astron. Soc.* **408** 2092
- [10] Di Piazza A, Müller C, Hatsagortsyan K Z and Keitel C H 2012 *Rev. Mod. Phys.* **84** 1177
- [11] Mackenroth F and di Piazza A 2011 *Phys. Rev. A* **83** 032106
- [12] Bulanov S S, Schroeder C B, Esarey E and Leemans W P 2013 *Phys. Rev. A* **87** 062110
- [13] Schwinger J 1951 *Phys. Rev.* **82** 664

- [14] Nerush E N, Kostyukov I Yu, Fedotov A M, Narozhny N B, Elkina N V and Ruhl H 2011 *Phys. Rev. Lett.* **106** 035001
- [15] Bula C *et al* 1996 *Phys. Rev. Lett.* **76** 3116
- [16] Burke D L *et al* 1997 *Phys. Rev. Lett.* **79** 1626
- [17] Andersen K K, Esberg J, Knudsen H, Thomsen H D, Uggerhøj U I, Sona P, Mangiarotti A, Ketel T J, Dizdar A and Ballestrero S 2012 *Phys. Rev. D* **86** 072001
- [18] Kneip S *et al* 2011 *Plasma Phys. Control. Fusion* **53** 014008
- [19] Kim H T, Pae K H, Cha H J, Kim I J, Yu T J, Sung J H, Lee S K, Jeong T M and Lee J 2013 *Phys. Rev. Lett.* **111** 165002
- [20] Wang X *et al* 2013 *Nat. Commun.* **4** 1988
- [21] Leemans W P *et al* 2014 *Phys. Rev. Lett.* **113** 245002
- [22] Chen S *et al* 2013 *Phys. Rev. Lett.* **110** 155003
- [23] Powers N D, Ghebregziabher I, Golovin G, Liu C, Chen S, Banerjee S, Zhang J and Umstadter D P 2013 *Nature Photon.* **8** 28
- [24] Sarri G *et al* 2014 *Phys. Rev. Lett.* **113** 224801
- [25] Sarri G *et al* 2015 *Nat. Comm.* **6** 6747
- [26] Yanovsky V *et al* 2008 *Opt. Express* **16** 2109
- [27] Thomas A G R, Ridgers C P, Bulanov S S, Griffin B J and Mangles S P D 2012 *Phys. Rev. X* **2** 041004
- [28] Neitz N and Di Piazza A 2013 *Phys. Rev. Lett.* **111** 054802
- [29] Mackenroth F, Neitz N and Di Piazza A 2013 *Plasma Phys. Control. Fusion* **55** 124018
- [30] Neitz N and Di Piazza A 2014 *Phys. Rev. A* **90** 022102
- [31] Ilderton A and Torgrimsson G 2013 *Phys. Lett. B* **725** 481
- [32] Green D G and Harvey C N 2014 *Phys. Rev. Lett.* **112** 164801
- [33] Li J X, Hatsagortsyan K Z and Keitel C H 2014 *Phys. Rev. Lett.* **113** 044801
- [34] Blackburn T G, Ridgers C P, Kirk J G and Bell A R 2014 *Phys. Rev. Lett.* **112** 015001
- [35] Erber T D 1966 *Rev. Mod. Phys.* **38** 4 626
- [36] Baier V N, Katkov V M and Strakhovenko V M 1998 *Electromagnetic Processes at High Energies in Oriented Single Crystals* (Singapore: World Scientific) p NNN
- [37] Ritus V I 1985 *J. Sov. Laser Res.* **6** 497
- [38] Furry W H 1951 *Phys. Rev.* **81** 115
- [39] Seipt D and Kämpfer B 2011 *Phys. Rev. A* **83** 022101
- [40] Heinzl T 2012 *Int. J. Mod. Phys. A* **27** 1260010
- [41] Mackenroth F and Di Piazza A 2013 *Phys. Rev. Lett.* **110** 070402
- [42] Ridgers C P, Kirk J G, Duclos R, Blackburn T G, Brady C S, Bennett K, Arber T D and Bell A R 2014 *J. Comp. Phys.* **260** 273
- [43] Elkina N V, Fedotov A M, Kostyukov I Yu, Legkov M V, Narozhny N B, Nerush E N and Ruhl H 2011 *Phys. Rev. ST Accel. Beams* **14** 054401
- [44] Landau L D and Lifshitz E M 1987 *The Course of Theoretical Physics* vol 2 (Oxford: Butterworth-Heinemann) p NNN
- [45] Boris J P 1970 *Proc. Fourth Conf. Num. Sim. Plasmas* (Washington DC: Naval Res. Lab.) p 3–67
- [46] Di Piazza A, Hatsagortsyan K Z and Keitel C H 2009 *Phys. Rev. Lett.* **102** 254802